materials

MDPI

Article

Thermo-Hydraulic Analysis of Heat Storage Filled with the Ceramic Bricks Dedicated to the Solar Air Heating System

Magdalena Nemś *, Artur Nemś, Jacek Kasperski and Michał Pomorski

Faculty of Mechanical and Power Engineering, Wroclaw University of Science and Technology, Wybrzeze Wyspianskiego 27, 50-370 Wroclaw, Poland; artur.nems@pwr.edu.pl (A.N.); jacek.kasperski@pwr.edu.pl (J.K.); michal.pomorski@pwr.edu.pl (M.P.)

* Correspondence: magdalena.nems@pwr.edu.pl; Tel.: +48-71-320-4826

Received: 28 June 2017; Accepted: 10 August 2017; Published: 12 August 2017

Abstract: This article presents the results of a study into a packed bed filled with ceramic bricks. The designed storage installation is supposed to become part of a heating system installed in a single-family house and eventually to be integrated with a concentrated solar collector adapted to climate conditions in Poland. The system's working medium is air. The investigated temperature ranges and air volume flow rates in the ceramic bed were dictated by the planned integration with a solar air heater. Designing a packed bed of sufficient parameters first required a mathematical model to be constructed and heat exchange to be analyzed, since heat accumulation is a complex process influenced by a number of material properties. The cases discussed in the literature are based on differing assumptions and different formulas are used in calculations. This article offers a comparison of various mathematical models and of system operating parameters obtained from these models. The primary focus is on the Nusselt number. Furthermore, in the article, the thermo-hydraulic efficiency of the investigated packed bed is presented. This part is based on a relationship used in solar air collectors with internal storage.

Keywords: heat storage; ceramic brick material; solar air space heating system

1. Introduction

Energy storage is becoming an increasingly important issue. The growing world economy causes an increased demand for energy in its various forms. Such situation has been long predicted, inter alia by Starr, who suggested, in the 1990s, a graph representing an increasing role that energy storage is going to play in the global energy balance between 1980 and 2016 [1]. According to the graph, stored energy should currently cover approximately 20% of global demand and its quantity should be comparable with the quantity of energy produced from conventional sources, such as coal. The same graph forecasts that, around 2040, stored energy should account for approximately 36% global demand.

Thermal energy storage (TES) systems are mainly coupled with sources of heat whose availability and intensity vary in time, i.e., mostly with renewable energy sources, and especially with solar energy systems. Heat storage is also used in industrial waste heat recovery systems. Although charging and discharging processes usually take place at the same location, mobile heat storage units are also sometimes used to deliver heat to demand sites located at distances of up to several kilometers [2].

Current research trends focus on phase change materials (PCM) as the most promising technology for heat energy accumulation processes [3]. Some works, as well as this article, are devoted to the issue of energy storage in sensible heat storage materials. Stone thermal storage units offer many advantages, including simple design and easy maintenance, low price, and safe operation. They can also work in a broad temperature range. Research into stone heat storage enjoyed much popularity in the 1980s

and 1990s, and resulted in many publications written at that time. This research explored inter alia the issue of pressure drop in packed beds with large-scale filling elements [4,5], experiments with a high-temperature accumulator (up to 700 °C) [6], and a solar thermal collector with internal rock bed storage [7]. Current research dedicated to sensible heat storage materials focuses on finding operating characteristics for packed beds having a particular design and on their specific industrial applications, e.g., as a storage system in a solar power plant [8,9] or in a greenhouse [10]. Solutions dedicated to building heating systems, e.g., to achieve level temperatures on a daily basis, are less frequently proposed [11].

Further part of the article offers the results of experiments on a packed bed filled with ceramic bricks. In the future, the bed is supposed to be charged with the air coming from a concentrated solar thermal collector system adapted to climate conditions in Poland (Figure 1). In the concept design of the heating system, the packed bed functions as a long-term heat storage unit located inside the building. The unit's planned volume is dedicated to a house constructed using energy-saving technology and is initially estimated at 8 m^3.

The choice of ceramic bricks as the filling material was dictated by several reasons. Structural stability can be provided more easily to a large bed filled with bricks than to a bed filled with, e.g., crushed stone or pebbles. Brick is also an easily available material and has good thermal properties. Additionally, brick is resistant to high temperatures and tolerates a high number of charge/discharge cycles. Brick does not emit any harmful gases in high temperatures, which is important, as the storage unit is to be located inside a residential house.

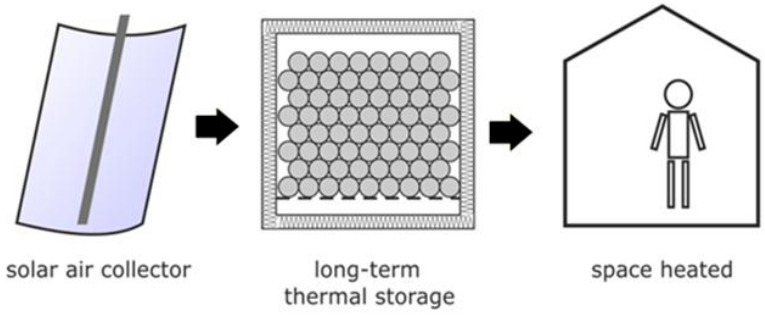

Figure 1. The concept of a solar heating system.

2. Thermo-Hydraulic Efficiency

The analysis of a rock heat storage system normally covers finding the amount of energy accumulated and the efficiency of the accumulation process. The authors of this article suggest that the charging process efficiency be calculated analogically to "η_{eff}— effective efficiency" (Equation (1)) proposed in 1990 by Cortes and Piacentini [12]:

$$\eta_{eff} = \frac{Q_u - \frac{p_m}{g}}{I \cdot A} \quad (1)$$

where Q_u is the useful heat gain, p_m is the mechanical energy consumed for propelling air through collector, g is the constant, I is the intensity of solar radiation and A is the area of absorber.

Mechanical energy consumption (p_m) for propelling air through the duct (Equation (2)) refers to mechanical energy loss due to flow resistance:

$$p_m = \frac{\dot{m} \cdot \Delta p}{\rho} = \dot{V} \cdot \Delta p \quad (2)$$

where $\dot{m}$ is the mass flow rate, Δp is the pressure drop across collector length and ρ is the density of fluid. Conversion efficiency g is calculated from the following relationship:

$$g = \eta_F \eta_E (1 - \zeta_t) \chi_c, \tag{3}$$

where η_F is the efficiency of the fan, η_E is the electric engine, ζ_t is the electric transmission loss coefficient and χ_c is the efficiency of thermal-electric conversion process. The assumed value was $g = 0.18$ in Argentina [12] and $g = 0.20$ in India [13]. This efficiency, nowadays more commonly referred to as the thermo-hydraulic efficiency, is frequently used in research papers as a means to analyze the work of solar air collectors with internal storage [14] or with additional elements improving heat exchange [15–17]. The relationship includes the amount of energy related to pressure drop in the system due to the flow resistance of the working medium.

The authors of this paper suggest that the thermo-hydraulic efficiency of the process of heat accumulation in a packed bed (η_{t-h}) be described with Equation (4), and be defined as: the ratio between the amount of energy absorbed by the packed bed $\dot{Q}_s$ minus the energy lost due to the flow resistance of the working medium in the packed bed and the total amount of energy $\dot{Q}_c$ which could be potentially absorbed by the packed bed:

$$\eta_{t-h} = \frac{\dot{Q}_s - \frac{\dot{V} \cdot \Delta p_c}{\eta_{fan}}}{\dot{Q}_c}, \tag{4}$$

where $\dot{Q}_s$ is the heat flux absorbed by the filler material of the packed bed, $\dot{V}$ is the volumetric flow rate, Δp_c is the total pressure drop in the system, η_{fan} is the efficiency of the fan and $\dot{Q}_c$ is the heat input flux. Conversion efficiency (Equation (3)) was replaced with the total efficiency of the fan. Its assumed value is 0.7.

3. Mathematical Model

Calculating thermo-hydraulic efficiency for the process of charging the packed bed required the construction of a mathematical model. The model involved balance calculations of heat input and heat output to/from the heat storage device with consideration to its geometry, as described in Figure 2. Each time step was assumed to be characterized by some steady conditions. The calculations were performed with the use of a steady heat exchange equation for each step. Table 1 shows the steady parameters assumed in the calculations.

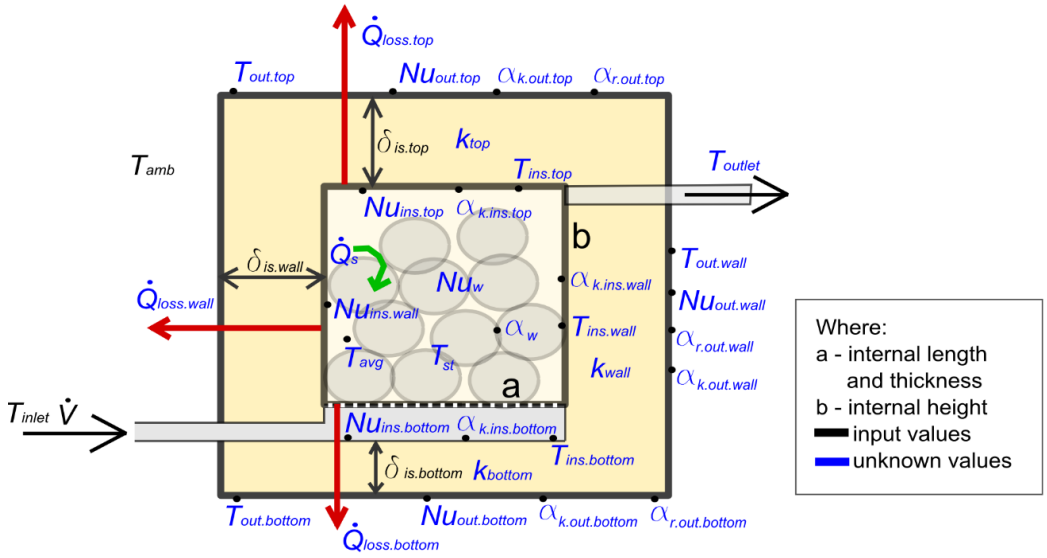

Figure 2. Scheme of the heat storage device with indicated input and calculation parameters.

Table 1. Input parameters used in the mathematical model.

Rock bed	Internal height	0.5 m
	Internal thickness	0.3 m
	Internal length	0.3 m
Storage material	Equivalent sphere diameter	0.149 m
	Specific heat	880 J/kgK
	Density	1800 kg/m^3
	Porosity	0.4
	Temperature in bed 1	18 °C
	Temperature in bed 2	28 °C
	Mass	40.16 kg
Air	Volumetric flow rate 1	0.0068 m^3/s
	Volumetric flow rate 2	0.0050 m^3/s
	Temperature inlet 1	220 °C
	Temperature inlet 2	100 °C
	Specific heat	f(T)
	Density	f(T)
	Kinematic viscosity	f(T)
	Ambient temperature	18 °C
Insulation	Top insulation thickness	0.20 m
	Bottom insulation thickness	0.15 m
	Side insulation thickness	0.15 m
	Specific heat	0.039 W/mK

Heat flux absorbed by the filler material of the packed bed ($\dot{Q}_s$) is equal to heat input flux ($\dot{Q}_c$) minus heat loss through the walls of the packed bed ($\dot{Q}_{loss}$). The accumulation process does not include heat output flux ($\dot{Q}_L$), which therefore has a value of zero in general Equation (5):

$$\dot{Q}_s = \dot{Q}_c - \dot{Q}_L - \dot{Q}_{loss}. \quad (5)$$

Equation (6) describes the heat input flux:

$$\dot{Q}_c = \dot{m} c_{p_{air}} (T_{inlet} - T_{outlet}), \quad (6)$$

where $\dot{m}$ is the mass flux of the air passing through the packed bed, $c_{p.air}$ is the heat proper of air at specific pressure, T_{inlet} is the air inlet temperature, and T_{outlet} is the air outlet temperature.

The flux of heat accumulated in the packed bed is described with Equation (7):

$$\dot{Q}_s = \frac{m_{st} \cdot c_{pst} \cdot \Delta T_{st}}{\tau}, \quad (7)$$

where m_{st} is the heat storage mass, c_{pst} is the specific heat of the filler material, and ΔT_{st} is the temperature rise in the packed bed. The accumulated heat flux is equal to the heat flux transferred to the filler material (Equation (8)):

$$\dot{Q}_s = \alpha_w \cdot S \cdot \left(T_{avg} - T_{st}\right), \quad (8)$$

where α_w is the heat-transfer coefficient, S is the area of the filler material, and T_{avg} is the average temperature, described with Equation (9):

$$T_{avg} = \frac{T_{inlet} + T_{outlet}}{2}. \quad (9)$$

The heat transfer coefficient is described with Equation (10):

$$\alpha = \frac{\lambda \cdot Nu}{x} \tag{10}$$

where λ is the thermal conductivity coefficient, Nu is the Nusselt number and x is the specific dimension. When calculating the coefficient of heat-transfer into the storage material α_w, specific parameter x was assumed to be D_{mat}, which is the diameter of a sphere having the same volume V_{mat} as the volume of a single brick, calculated as in Equation (11).

$$D_{mat} = \sqrt[3]{\frac{6 \cdot V_{mat}}{\pi}} \tag{11}$$

Equation (10) served to establish the coefficient of heat transfer from the air passing inside the packed bed to the surface of the bed walls. Specific parameter x used to establish $\alpha_{k.ins.wall}$ was the height of the packed bed b, while the characteristic parameter used to establish $\alpha_{k.ins.top}$ and $\alpha_{k.ins.bottom}$ was the width of the packed bed a.

Equation (10) was also used to find the convective heat-transfer coefficient on the inside of the storage device $\alpha_{k.out}$. The $\alpha_{k.out.wall}$ was calculated from $x = b + 2 \cdot \delta_{is.top-bottom}$, while the $\alpha_{k.out.top}$ and $\alpha_{k.out.bottom}$ were calculated from $x = a + 2 \cdot \delta_{is.wall}$.

Nusselt number is the function of Reynolds number (Re) and Prandtl number (Pr):

$$Nu_w = A \cdot Re^B \cdot Pr^C. \tag{12}$$

Constants A, B, and C in this formula describe the process of heat transfer into the filler material of the storage device.

Formula (13) describes the heat loss flux from the packed bed:

$$\dot{Q}_{loss} = (k \cdot A) \cdot (T_{avg} - T_{amb}), \tag{13}$$

where k is the overall heat transfer coefficient, A is the area, and T_{amb} is the ambient temperature.

After including the area of heat loss from the packed bed, the formula becomes Equation (14):

$$\begin{aligned} \dot{Q}_{loss} = \dot{Q}_{loss.top} + \dot{Q}_{loss.bottom} + \dot{Q}_{loss.wall} = \left[k_{top}\left(a + 2\delta_{is_{wall}}\right)^2 + k_{bottom}\left(a + 2\delta_{is_{wall}}\right)^2\right] \\ + k_{wall} \cdot \left[4 \cdot \left(a + 2\delta_{is_{wall}}\right) \cdot b + \left(2\delta_{is_{top-bottom}}\right)\right]\left(T_{avg} - T_{amb}\right). \end{aligned} \tag{14}$$

Equations (7), (8) and (14) served to find heat transfer flux $\dot{Q}_s$ and temperatures: T_{outlet} and T_{st}.

After Equations (6) and (14) were substituted into Equation (5), the result was:

$$\begin{aligned} \dot{Q}_s = \dot{m} c_p (T_{inlet} - T_{outlet}) - \left[k_{wall} \cdot \left[4 \cdot \left(a + 2\delta_{is_{wall}}\right) \cdot \left(b + 2\delta_{is_{top-bottom}}\right)\right]\right. \\ \left. + k_{bottom}\left(a + 2\delta_{is_{wall}}\right)^2 + k_{top}\left(a + 2\delta_{is_{wall}}\right)^2\right]\left(T_{avg} - T_{amb}\right). \end{aligned} \tag{15}$$

The overall coefficients of heat transfer through the housing of the packed bed are calculated from Equation (16) [18]:

$$k = \frac{1}{\frac{1}{\alpha_k} + \frac{\delta_{wall1}}{\lambda_{wall1}} + \frac{\delta_{is}}{\lambda_{is}} + \frac{\delta_{wall2}}{\lambda_{wall2}} + \frac{1}{\alpha_k + \alpha_r}}, \tag{16}$$

where α_k is the convective heat-transfer coefficient, and α_r is the radiant heat-transfer coefficient.

To find the coefficient of heat transfer through the side wall k_{wall}, three coefficients were used: the coefficient of heat transfer on the inside wall $\alpha_{k.ins.wall}$, as well as the convective coefficient $\alpha_{k.out.wall}$ and the radiant coefficient on the outside wall. Due to its negligible influence on the obtained heat flux, the resistance caused by the steel sheet used in the housing of the packed bed was disregarded

$\frac{\delta_{wall1}}{\lambda_{wall1}}$ and $\frac{\delta_{wall2}}{\lambda_{wall2}}$—value δ_{is} was substituted with $\delta_{is.wall}$ and λ_{is} of the insulating material. The same procedure was performed for the top surface, whose coefficient k_{top} was calculated by substituting $\alpha_{k.ins.top}$, $\alpha_{k.out.top}$, $\alpha_{r.out.top}$ and by assuming insulation thickness $\delta_{is.top\text{-}bottom}$ and for the bottom surface, in which k_{bottom} depended on $\alpha_{k.ins.bottom}$, $\alpha_{k.out.bottom}$, $\alpha_{r.out.bottom}$ and on insulation thickness $\delta_{is.top-bottom}$.

Convective heat-transfer coefficient is calculated as in Equation (10), while radiant heat-transfer coefficient is calculated from Equation (17):

$$\alpha_r = \frac{\varepsilon_{wall} \cdot \sigma \cdot \left(T_{out}^4 - T_{amb}^4\right)}{T_{out} - T_{amb}}, \tag{17}$$

where ε_{wall} is the emissivity of the plate, σ is the Stefan–Boltzmann constant and T_{out} is the temperature of the packed bed's outside surface. The radiant coefficient of heat absorption from the side wall $\alpha_{r.out.wall}$ was calculated by assuming surface temperature $T_{out.wall}$. Coefficients $\alpha_{r.out.top}$ and $\alpha_{r.out.bottom}$ were calculated by assuming temperatures $T_{out.top}$ and $T_{out.bottom}$, respectively.

An assumption was made that on the outside wall of the storage device's housing, heat is transferred by radiance described with Formula (17) and by natural convection. Therefore, the convective heat-transfer coefficient on the outside of the packed bed was calculated from the relationship between Nusselt number and Prandtl and Grashoff numbers (Equation (18)):

$$Nu_{out} = C \cdot (Gr \cdot Pr)^n, \tag{18}$$

where according to Kostowski [19]:

$Gr \cdot Pr < 10^{-3}$, $C = 0.5$, $n = 0$
$10^{-3} < Gr \cdot Pr < 500$, $C = 1.18$, $n = 1/8$
$500 \leq Gr \cdot Pr < 2 \cdot 10^7$, $C = 0.54$, $n = 1/4$
$2 \cdot 10^7 \leq Gr \cdot Pr$, $C = 0.135$, $n = 1/3$.

For such case, the Grashoff number was calculated from Equation (19):

$$Gr = \frac{g \cdot x^3 \frac{1}{d\frac{T_{amb}+T_{out}}{2}} \left(T_{out} - T_{amb}\right)}{\nu^2}, \tag{19}$$

where g is the gravitational acceleration, x is the specific dimension, and ν is the coefficient of kinematic viscosity.

The Nusselt number was established for the outside surface of the side wall $Nu_{out.wall}$ by assuming specific dimension x to be $b + 2 \cdot \delta_{is.top\text{-}bottom}$ and the temperature of the outside surface to be $T_{out.wall}$. At the same time, $Nu_{out.top}$ was calculated by assuming x to be $a + 2 \cdot \delta_{is.wall}$ and the temperature of the outside surface to be $T_{out.top}$, and the assumptions for the bottom surface were analogically $x = a + 2 \cdot \delta_{is.wall}$ and temperature $T_{out.bottom}$.

The convective heat-transfer coefficient on the inside of the storage device was calculated from the Nu_{ins} Equation (20) [19] describing heat transfer during laminar flow around the plate:

$$Nu_{ins} = 0.593 \cdot Re^{0.5}, \tag{20}$$

where, for the sidewall surface, the value of $Nu_{ins.wall}$ was established by substituting specific parameter x with internal height of the bed b, and to calculate the Nusselt number for the top surface $Nu_{ins.top}$ and for the bottom surface $Nu_{ins.bottom}$, x was substituted with base length a.

The model included calculations made to ensure that the assumed temperatures on the walls of the housing are correct. The flux of heat loss through each of the housing layers was assumed to be constant:

$$\dot{Q}_{loss} = \left(T_{avg} - T_{ins}\right) \cdot \alpha_{k_{ins}} \cdot A_{ins}, \tag{21}$$

$$\dot{Q}_{loss} = (T_{out} - T_{amb}) \cdot (\alpha_{k.out} + \alpha_{r.out}) \cdot \frac{A_{ins} + A_{out}}{2}, \quad (22)$$

$$\dot{Q}_{loss} = (T_{ins} - T_{out}) \cdot \left(\frac{\delta_{wall1}}{\lambda_{wall1}} + \frac{\delta_{is}}{\lambda_{is}} + \frac{\delta_{wall2}}{\lambda_{wall2}} \right) \cdot A_{out}, \quad (23)$$

where T_{ins} is the temperature of the wall on the inside, A_{ins} is the area of the inside wall and A_{out} is the temperature of the wall on the outside. A_{ins} for the sidewall surface was described as $A_{ins.wall} = 4 \cdot a \cdot b$, and A_{out} as $A_{out.wall} = 4 \cdot (a + 2 \cdot \delta_{is.wall}) \cdot (b + 2 \cdot \delta_{is.top.bottom})$. Meanwhile, A_{ins} for the top and bottom surface was describe as $A_{in.top.bottom} = a^2$, and A_{out} as $A_{out.top.bottom} = (a + 2 \cdot \delta_{ins.wall})^2$.

Equations (21)–(23) were used to find heat loss fluxes from sidewall, top and bottom surfaces of the packed bed. Values T_{ins}, T_{out}, $\alpha_{k.ins}$, $\alpha_{k.out}$, $\alpha_{r.out}$ and δ_{is} for each surface were assumed in accordance with the labels in Figure 2, forming a set of nine equations (three per a loss flux in each direction: $\dot{Q}_{loss.wall}$, $\dot{Q}_{loss.botttom}$, and $\dot{Q}_{loss.top}$), which allow the calculation of unknown loss fluxes, $\dot{Q}_{loss.wall}$, $\dot{Q}_{loss.botttom}$, and $\dot{Q}_{loss.top}$, and of the temperatures on the walls of the bed, $T_{ins.wall}$, $T_{out.wall}$, $T_{ins.bottom}$, $T_{out.bottom}$, $T_{ins.top}$, and $T_{out.top}$.

The working medium was air considered as a semi ideal gas. A set was obtained of 33 balance equations and 33 unknown values. The unknown values are:

- temperatures: T_{outlet}, T_{st}, T_{avg}, $T_{ins.wall}$, $T_{out.wall}$, $T_{ins.bottom}$, $T_{out.bottom}$, $T_{ins.top}$, and $T_{out.top}$;
- heat fluxes: $\dot{Q}_s$, $\dot{Q}_{loss.wall}$, $\dot{Q}_{loss.botttom}$, and $\dot{Q}_{loss.top}$;
- the Nu numbers: Nu_w, $Nu_{out.wall}$, $Nu_{ins.wall}$, $Nu_{ins.bottom}$, $Nu_{out.bottom}$, $Nu_{ins.top}$, and $Nu_{out.top}$;
- heat-transfer coefficients: α_w, $\alpha_{k.out.wall}$, $\alpha_{k.ins.wall}$, $\alpha_{r.out.wall}$, $\alpha_{k.ins.bottom}$, $\alpha_{k.out.bottom}$, $\alpha_{r.out.bottom}$, $\alpha_{k.ins.top}$, $\alpha_{k.out.top}$, and $\alpha_{r.out.top}$; and
- overall heat transfer coefficients: k_{wall}, k_{bottom}, and k_{top}.

To provide an iterative solution to this system of equations, commercially available Mathcad 15.0 software was used.

The effectiveness of the accumulation process should include pressure drop in the system, which is related to the flow resistance due to the shape and the filling factor of the packed bed, analogically to the calculations for a solar thermal collector [20,21]. To find total pressure drop Δp_c using the packed bed's measurement system, it was necessary to calculate the pressure drop in the bed itself and in the outlet channel, as well as the local pressure drop due to the system's geometry. Friction loss factor in the packed bed f_m [14] is described by Equation (24):

$$f_m = 150 \cdot \left[\frac{1 - \varepsilon_{st}}{Re_{st}} \right] + 1.75 \quad (24)$$

where ε_{st} is the filling factor of the packed bed with air. Its solution required calculating the Reynolds number for the flow of the working medium through the packed bed, from Formula (25):

$$Re_{st} = \frac{D_e \cdot \rho_{air} \cdot w}{\mu}, \quad (25)$$

where D_e is the specific dimension of the filler material, w is the flow velocity of the working medium and μ is the coefficient of dynamic viscosity. The filler material's specific dimension D_e [14] is:

$$D_e = \frac{2}{3} \cdot \frac{\varepsilon_{st} \cdot D_{mat}}{1 - \varepsilon_{st}}, \quad (26)$$

The D_e dimension used in the pressure drop formulas included equivalent diameter of the filler material D_{mat}. According to the literature, the equivalent diameter of the filler material can be approximated by the diameter of a sphere. Therefore, its calculation required finding the mass of

bricks and counting the number of filler elements. The filling factor of the packed bed with air, which is required to solve Equation (22), can be calculated from Equation (27) [14]:

$$\varepsilon_{st} = \frac{V_c - nV_{mat}}{V_c}, \tag{27}$$

where V_c is the total bed volume.

Pressure drop in the bed, which results from transforming the formulas provided in [14,22], is described by:

$$\Delta p_{st} = \frac{2 \cdot \rho_{air} \cdot f_m \cdot \dot{V}^2 \cdot b \cdot (1 - \varepsilon_{st})}{B^2 \cdot D_e \cdot \varepsilon_{st}^3}, \tag{28}$$

where B is the bed's section area and b is the bed's height. Calculating pressure drop in the outlet channel firstly required finding the Reynolds number, according to Equation (29):

$$Re_k = \frac{\rho_{air} \cdot v_k \cdot D_k}{\mu}, \tag{29}$$

where v_k is the velocity in the channel, and D_k is the diameter of the channel. The next step consisted in using the friction coefficient ξ formula, which was assumed for the turbulent flow, according to Blasius formula [23]:

$$\xi = \frac{0.316}{Re_k^{0.25}}. \tag{30}$$

Pressure loss due to friction during turbulent flow through a straight duct of any and uniform section, as described with the Darcy–Weisbach relationship [24], is defined as:

$$\Delta p_k = \xi \cdot \frac{L_k \cdot v_k^2 \cdot \rho_{air}}{4 \cdot R_h \cdot 2}, \tag{31}$$

where L_k is the length of the duct, and R_h is the hydraulic diameter.

In order to calculate local pressure drop due to the change of the shape and direction of flow, first it is necessary to assume a local resistance coefficient. According to tables provided in [25], a coefficient was selected for an elbow pipe with additional change of the section area of the elements: ζ = 1.24. Local pressure loss should be in this case proportional to the dynamic pressure of the fluid stream (31):

$$\Delta p_m = \zeta \cdot \frac{v_{śr}^2 \cdot \rho_p}{2}. \tag{32}$$

Thus, the total pressure drop in the system is described by Equation (33):

$$\Delta p_c = \Delta p_{st} + \Delta p_k + \Delta p_m. \tag{33}$$

The Nusselt Number

The literature offers many formulas for calculating the Nusselt number for the flow around the storage material. Out of the available mathematical formulas, the authors chose to use those which had been applied for the filler material in the form of spheres, or which had an equivalent diameter calculated. In each of the cases, the working medium was air, considered as a semi ideal gas, for which the assumed Prandtl number was 0.7. Table 2 shows eight formulas along with their conditions of use (if such had been provided).

Table 2. Selected Nusselt number formulas.

No.	Dimensionless Equation		Notes	Reference
1	$Nu_w = 2 + 0.6 \cdot Re^{0.5} \cdot Pr^{1/3}$	(34)	$1 \leq \mathrm{Re} \leq 70{,}000$ $0.6 \leq \mathrm{Pr} \leq 400$	[19]
2	$Nu_w = 0.8 \cdot Re^{0.7} \cdot Pr^{0.33}$	(35)	$500 \leq \mathrm{Re} \leq 50{,}000$	[19]
3	$Nu_w = 2 + 0.03 \cdot Re^{0.54} \cdot Pr^{\frac{1}{33}} + 0.35 \cdot Re^{0.58} \cdot Pr^{0.356}$	(36)	-	[26]
4	$Nu_w = 2 + 1.8 \cdot Re^{0.5} \cdot Pr^{1/3}$	(37)	$100 \leq \mathrm{Re}$ Pr for typical gases and liquids	[26]
5	$Nu_w = 2 + 1.1 \cdot Re^{0.6} \cdot Pr^{1/3}$	(38)	$15 \leq \mathrm{Re} \leq 8500$	[27]
6	$Nu_w = 0.29 \cdot Re^{0.8} \cdot Pr^{1/2}$	(39)	$\mathrm{Re} \leq 2400$	[28]
7	$Nu_w = 2 + 1.354 \cdot Re^{\frac{1}{2}} \cdot Pr^{\frac{1}{3}} + 0.0326 \cdot Re \cdot Pr^{1/2}$	(40)	$60 \leq \mathrm{Re}$	[29]
8	$Nu_w = 0.437 \cdot Re^{0.75} \cdot \psi^{3.35} \cdot \varepsilon^{-1.62} \cdot \left[exp\left\{ 29.03 (log\psi)^2 \right\} \right]$	(41)	$\varepsilon = \frac{V_b - V_s}{V_b}$ * $\psi = \frac{a_s}{a_c}$ **	[30]

* ε is the filling factor of the packed bed with air, V_b is the bed volume and V_s is the volume of the filler material;
** ψ is the area ratio, as is the area of the sphere and ac is the area of the brick.

With the same boundary conditions selected, the above formulas provide different results. By comparing the results of actual experiments with the results from mathematical models, it will be possible to indicate the formula which best characterizes the process of thermal energy storage in ceramic bricks.

4. Experimental Set-Up

Figure 3 shows the experimental set-up used in the experiments on the process of heat storage. The experimental set-up comprises two metal, cuboid-shaped housings, with mineral wool inserted between them. The chosen filler material is placed in the inner housing. Both housings are made of zinc coated sheets between 1 mm and 3 mm in thickness. The remaining dimensions and operating parameters of the packed bed are provided in Table 1.

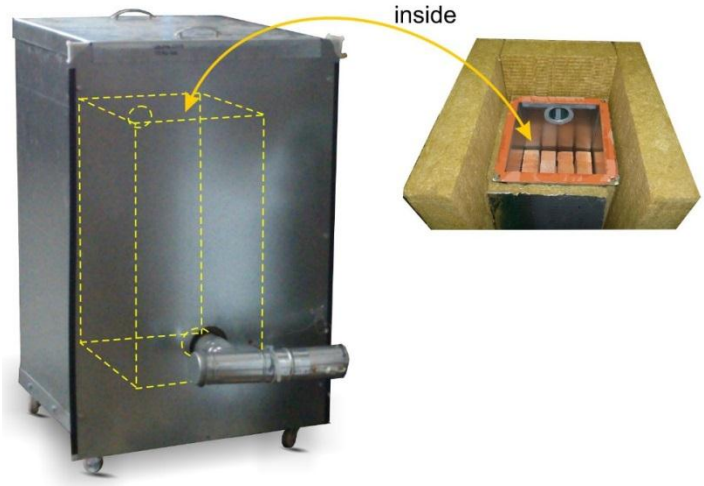

Figure 3. Experimental set-up for examining heat storage process in the rock bed.

4.1. The Operating Principle and the Measuring Apparatus

Figure 4 shows a schematic diagram of the experimental set-up with the measuring apparatus.

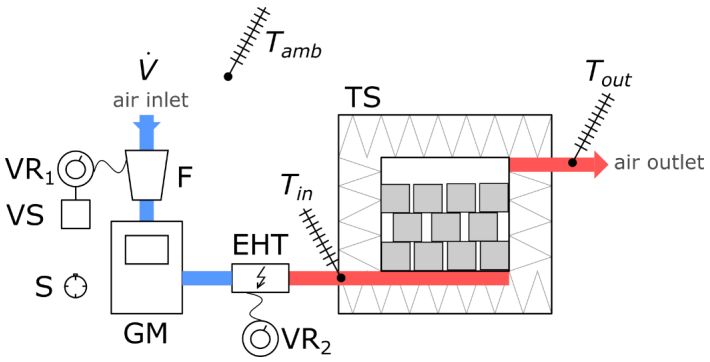

Figure 4. Schematic diagram of the experimental set-up for examining heat storage process.

Air stream $\dot{V}$ is forced into the system with fan F. The fan is powered by autotransformer VR1, which allows changing the stream of the flowing air. Autotransformer VR1 is additionally connected to voltage regulator VS. The air then flows through gas flowmeter GM, which allows reading the volume of the flowing medium over time measured by stop watch S. The air forced by fan F flows through electric heater EHT having a maximum power of 1.7 kW, powered from autotransformer VR2. This allows regulating inlet temperature T_{in}. The settings of VR2 are determined experimentally and depend on the stream of airflow and on ambient temperature T_{amb}. In order to flatten the velocity field, warmed airflows into packed bed TS through symmetrically distributed intake apertures, where it gives off heat to the filler material. Cooled air having temperature T_{out} flows through an outlet channel located in the upper part of packed bed TS and is dissipated in the environment. The system is open-cycle.

Temperature measurement is performed with K-type thermocouples. The measured temperatures include: ambient temperature T_{amb}, inlet temperature T_{in} and outlet temperature T_{out}. The results were recorded at 60-s intervals on Lumel KD7 automatic data logger.

4.2. Experimental Tests and Uncertainty Analysis

The tests of heat storage process in ceramic brick were performed for two airflow rates and two different inlet temperatures. Both the airflow stream and the values of temperatures at the inlet of the medium to the packed bed were selected from a perspective of integrating the packed bed with a concentrated solar collector as part of a heating system installed in a single-family house. The parameters were selected previously, according to the analyses of the solar heater, as offered in [20,21].

Initial parameters for the first and for the second experiment are shown in Table 2. Ambient temperature for both measurements was 18 °C. In the second experiment, for a smaller airflow, the charging process was performed on the packed bed which was not fully discharged. The temperature of the packed bed was 28 °C, which corresponds to conditions frequently encountered in the target system. During the experiments, the end of the heat storage process was marked by the absolute increment of outlet temperature over the 10-minute period being $\Delta T < 2$ °C for the first airflow, and $\Delta T < 1$ °C for the second airflow.

Figure 5 illustrates the changes in the outlet temperature of air over time. The significantly different values of temperature at the inlet to the packed bed result in considerably different dynamics of the process of heat absorption by the packed bed in the first hour of the process. This fact is of importance for the construction of a model which will accurately represent the character of the process. The shape of the characteristic curve in the first hour of the charging process is of great importance also because of the planned integration of the packed bed with the heating system, where the period of time over which a certain level of direct solar radiation is available will determine the temperature at the inlet to the packed bed.

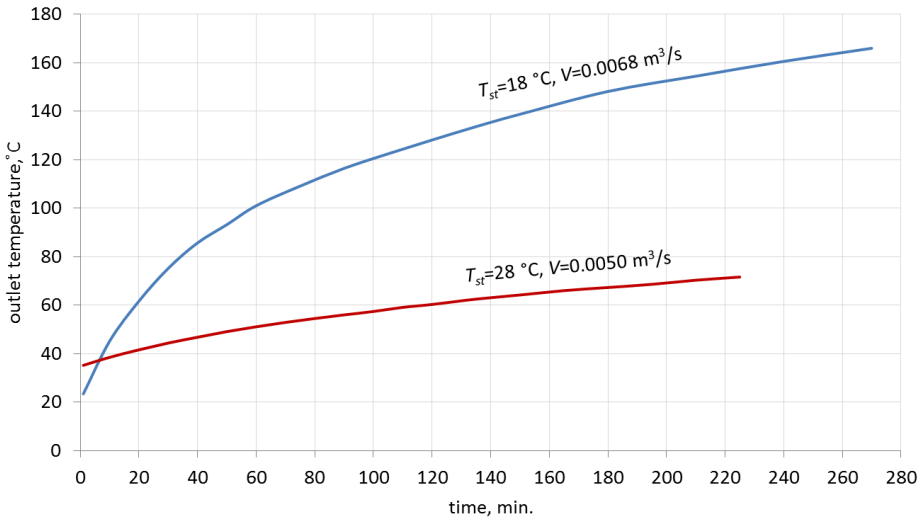

Figure 5. Change of outlet temperature as a function of charging time for two examined airflow rates.

After the experiments had been completed, the results were subjected to uncertainty analysis. The uncertainty of determining the thermo-hydraulic efficiency can be tested with the analysis of the measuring accuracy of the equipment used. The analysis of uncertainty for the equipment used in calculation of such parameters as temperature, volume flux and pressure drop was done according to the procedures described in [31]. For the calculated extended uncertainties, a coverage factor of 2 was adopted. Uncertainties, specified by the manufacturers, are: 0.1 °C for temperature, 1% for airflow in m^3/s and 0.5 Pa for pressure drop measurement. Values of uncertainty bars were added to the characteristics represented in the next Chapter.

5. Model Validation

The results obtained from the balance equations described in Section 3 were compared with the results of experiments. The model included the boundary conditions obtained in experiments and the outlet temperature served as the comparative parameter. The results of analytical calculations were generated for all eight of the Nusselt number formulas. To validate the results, Equation (42) was used, which describes the deviation of outlet air temperature values obtained from the model in relation to the values obtained in the experiments:

$$\delta T_{out} = \left| \frac{T_{out} - T_{out.m}}{T_{out}} \right| \cdot 100, \ \% . \tag{42}$$

Tables 3 and 4 show the results for the airflow of 0.0050 m^3/s. Tables 5 and 6 shows the results for the airflow of 0.0068 m^3/s. The results are presented graphically in Figures 6 and 7, respectively.

When analyzing the obtained results, one can observe that for the airflow of 0.0050 m^3/s, the deviations of outlet temperature are significantly lower than for the airflow of 0.0068 m^3/s. In the case of formula No. 1 (see Table 2), the deviations are up to 72.2% for the first airflow and up to 223.7% for the second airflow.

Figures 6 and 7 show that outlet temperatures for 6 dimensionless equations of the *Nu* number are similar to experiment results. Outlet temperatures obtained from models based on formulas Nos. 1 and 3 show the changes of outlet temperature to have a completely different character.

The results obtained for formula No. 2 were closest to the experimentally obtained results. Applying this formula for the airflow of 0.0050 m^3/s resulted in the average deviation of 2.2%, the maximum deviation of 3.6%, and the minimum deviation of 0.4%. In the case of the airflow of 0.0068 m^3/s, these deviations were much greater: average of 3.5%, maximum of 13.2%, and minimum of 0%. Since formula No. 2 was assumed to sufficiently represent the character of changes in the analyzed process, it was selected for further analysis.

Table 3. Experiment results for the airflow of 0.0050 m^3/s.

Experiment			Models							
			No. 1	No. 2	No. 3	No. 4	No. 5	No. 6	No. 7	No. 8
No.	t	T_{out}	T_{out}	T_{out}	T_{out}	T_{out}	T_{out}	T_{out}	T_{out}	T_{out}
	min	°C	°C	°C	°C	°C	°C	°C	°C	°C
1	1	35.2	60.6	34.3	59.8	40.6	38.1	39.8	37.7	42.4
2	10	38.5	61.8	37.1	61.0	43.2	41.0	42.7	40.6	45.1
3	20	41.6	63.0	40.4	62.2	46.4	44.1	45.7	43.8	47.9
4	30	44.4	64.2	43.6	63.5	49.1	47.0	48.5	46.7	50.5
5	40	46.8	65.2	46.6	64.6	51.5	49.7	51.0	49.4	52.8
6	50	49.1	66.2	49.3	65.7	53.7	52.1	53.3	51.9	54.9
7	60	51.1	67.1	51.8	66.5	55.5	54.3	55.3	54.0	56.8
8	70	52.9	68.0	54.0	67.5	57.6	56.2	57.2	56.0	58.5
9	80	54.5	68.8	56.0	68.4	59.2	58.0	58.9	57.8	60.1
10	90	56.0	69.5	57.8	69.1	60.7	59.6	60.4	59.3	61.5
11	100	57.4	70.2	59.4	69.9	62.1	61.1	61.8	61.0	62.8
12	110	59.1	70.9	60.9	70.6	63.4	62.5	63.1	62.3	64.0
13	120	60.3	71.5	62.3	71.2	64.5	63.7	64.3	63.6	65.2
14	135	62.5	72.4	64.2	72.1	66.1	65.4	65.9	65.3	66.7
15	150	64.2	73.2	65.8	73.0	67.5	66.9	67.4	66.8	68.0
16	165	66.0	74.0	67.3	73.8	68.8	68.3	68.7	68.2	69.3
17	180	67.3	74.7	68.6	74.5	70.0	69.5	69.9	69.4	70.4
18	195	68.6	75.4	69.8	75.2	71.1	70.6	71.0	70.5	71.4
19	210	70.3	76.0	70.9	75.9	72.0	71.6	71.9	71.6	72.4
20	225	71.6	76.6	71.9	76.4	72.9	72.6	72.9	72.5	73.3

Table 4. Deviations for the airflow of 0.0050 m^3/s.

Experiment			Models							
			No. 1	No. 2	No. 3	No. 4	No. 5	No. 6	No. 7	No. 8
No.	t	T_{out}	δT_{out}	δT_{out}	δT_{out}	δT_{out}	δT_{out}	δT_{out}	δT_{out}	δT_{out}
	min	°C	%	%	%	%	%	%	%	%
1	1	35.2	72.2	2.6	69.9	15.3	8.2	13.1	7.1	20.5
2	10	38.5	60.5	3.6	58.4	12.2	6.5	10.9	5.5	17.1
3	20	41.6	51.4	2.9	49.5	11.5	6.0	9.9	5.3	15.1
4	30	44.4	44.6	1.8	43.0	10.6	5.9	9.2	5.2	13.7
5	40	46.8	39.3	0.4	38.0	10.0	6.2	9.0	5.6	12.8
6	50	49.1	34.8	0.4	33.8	9.4	6.1	8.6	5.7	11.8
7	60	51.1	31.3	1.4	30.1	8.6	6.3	8.2	5.7	11.2
8	70	52.9	28.5	2.1	27.6	8.9	6.2	8.1	5.9	10.6
9	80	54.5	26.2	2.8	25.5	8.6	6.4	8.1	6.1	10.3
10	90	56.0	24.1	3.2	23.4	8.4	6.4	7.9	5.9	9.8
11	100	57.4	22.3	3.5	21.8	8.2	6.4	7.7	6.3	9.4
12	110	59.1	20.0	3.0	19.5	7.3	5.8	6.8	5.4	8.3
13	120	60.3	18.6	3.3	18.1	7.0	5.6	6.6	5.5	8.1
14	135	62.5	15.8	2.7	15.4	5.8	4.6	5.4	4.5	6.7
15	150	64.2	14.0	2.5	13.7	5.1	4.2	5.0	4.0	5.9
16	165	66.0	12.1	2.0	11.8	4.2	3.5	4.1	3.3	5.0
17	180	67.3	11.0	1.9	10.7	4.0	3.3	3.9	3.1	4.6
18	195	68.6	9.9	1.7	9.6	3.6	2.9	3.5	2.8	4.1
19	210	70.3	8.1	0.9	8.0	2.4	1.8	2.3	1.8	3.0
20	225	71.6	7.0	0.4	6.7	1.8	1.4	1.8	1.3	2.4
deviation %		avg.	27.6	2.2	26.7	7.7	5.2	7.0	4.8	9.5
		max.	72.2	3.6	69.9	15.3	8.2	13.1	7.1	20.5
		min.	7.0	0.4	6.7	1.8	1.4	1.8	1.3	2.4

Table 5. Experiment for the airflow of 0.0068 m^3/s.

Experiment			Models							
			No. 1	**No. 2**	**No. 3**	**No. 4**	**No. 5**	**No. 6**	**No. 7**	**No. 8**
No.	t	T_{out}	T_{out}	T_{out}	T_{out}	T_{out}	T_{out}	T_{out}	T_{out}	T_{out}
	min	**°C**	**°C**	**°C**	**°C**	**°C**	**°C**	**°C**	**°C**	**°C**
1	1	23.4	75.7	26.5	74.0	40.7	34.9	36.2	33.4	41.5
2	10	45.2	114.3	43.0	111.9	63.8	55.7	58.6	53.8	66.1
3	20	61.7	129.6	59.9	127.3	80.2	72.5	75.7	70.8	82.9
4	30	75.2	133.6	72.7	131.6	90.2	83.6	86.5	82.1	92.7
5	40	85.7	137.1	83.9	135.4	98.9	93.2	95.8	92.0	101.2
6	50	93.2	140.4	93.5	138.8	106.5	101.6	103.9	100.6	108.6
7	60	101.0	143.3	101.9	141.9	113.1	108.9	110.9	108.0	115.0
8	75	109.1	147.3	112.5	146.1	121.7	118.2	119.9	117.5	123.3
9	90	116.4	150.8	121.2	149.8	128.8	125.9	127.4	125.3	130.2
10	105	122.4	153.9	128.5	153.0	134.8	132.4	133.7	131.9	136.0
11	120	128.1	156.6	134.6	155.9	140.0	137.9	139.0	137.5	141.1
12	135	133.6	159.1	139.8	158.4	144.5	142.7	143.6	142.3	145.4
13	150	138.7	161.3	144.3	160.8	148.4	146.8	147.6	146.5	149.2
14	180	148.1	165.2	151.7	164.8	154.8	153.6	154.2	153.4	155.4
15	210	154.4	168.4	157.4	168.1	159.9	159.0	159.5	158.8	160.5
16	240	160.5	171.1	162.1	170.9	164.1	163.3	163.7	163.2	164.5
17	270	165.9	173.5	165.9	173.3	167.5	166.9	167.2	166.8	167.9

Table 6. Deviations for the airflow of 0.0068 m^3/s.

Experiment			Models							
			No. 1	**No. 2**	**No. 3**	**No. 4**	**No. 5**	**No. 6**	**No. 7**	**No. 8**
No.	t	T_{out}	δT_{out}	δT_{out}	δT_{out}	δT_{out}	δT_{out}	δT_{out}	δT_{out}	δT_{out}
	min	**°C**	**%**	**%**	**%**	**%**	**%**	**%**	**%**	**%**
1	1	23.4	223.7	13.2	216.2	74.1	49.2	54.9	42.6	77.3
2	10	45.2	152.8	4.9	147.6	41.1	23.3	29.6	19.0	46.2
3	20	61.7	110.0	2.8	106.4	30.0	17.5	22.6	14.7	34.4
4	30	75.2	77.6	3.3	74.9	19.9	11.1	15.0	9.2	23.3
5	40	85.7	60.0	2.1	58.0	15.4	8.8	11.8	7.3	18.1
6	50	93.2	50.6	0.4	48.9	14.3	9.0	11.5	7.9	16.5
7	60	101.0	41.9	0.9	40.5	12.0	7.8	9.8	7.0	13.9
8	75	109.1	35.0	3.2	33.9	11.5	8.3	9.9	7.7	13.0
9	90	116.4	29.5	4.2	28.7	10.7	8.2	9.4	7.7	11.8
10	105	122.4	25.7	5.0	25.0	10.2	8.2	9.2	7.8	11.1
11	120	128.1	22.3	5.1	21.7	9.3	7.7	8.5	7.4	10.1
12	135	133.6	19.1	4.7	18.6	8.1	6.8	7.5	6.5	8.8
13	150	138.7	16.3	4.1	15.9	7.0	5.8	6.4	5.6	7.5
14	180	148.1	11.5	2.4	11.2	4.5	3.7	4.1	3.6	5.0
15	210	154.4	9.1	2.0	8.9	3.6	2.9	3.3	2.8	3.9
16	240	160.5	6.6	1.0	6.5	2.2	1.7	2.0	1.7	2.5
17	270	165.9	4.6	0.0	4.5	1.0	0.6	0.8	0.5	1.2
deviation %		avg.	52.7	3.5	51.0	16.2	10.6	12.7	9.3	17.9
		max.	223.7	13.2	216.2	74.1	49.2	54.9	42.6	77.3
		min.	4.6	0.0	4.5	1.0	0.6	0.8	0.5	1.2

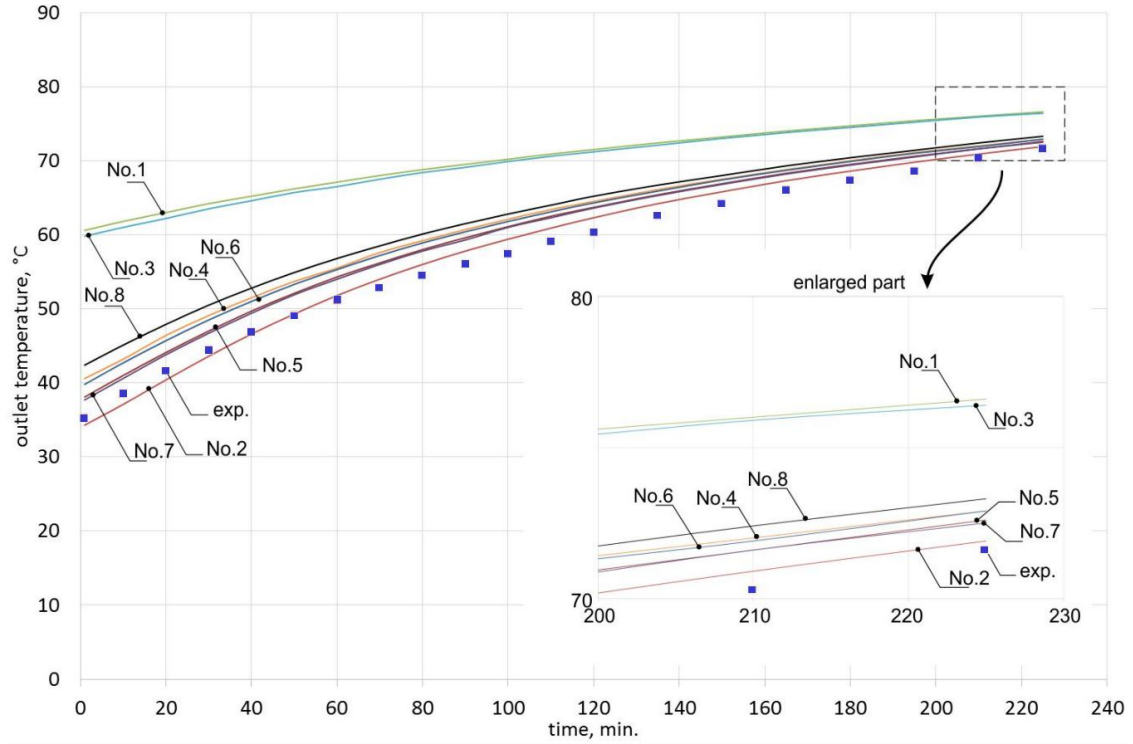

Figure 6. Outlet temperature for the airflow of 0.0050 m^3/s, for each of the dimensionless equations from Table 2.

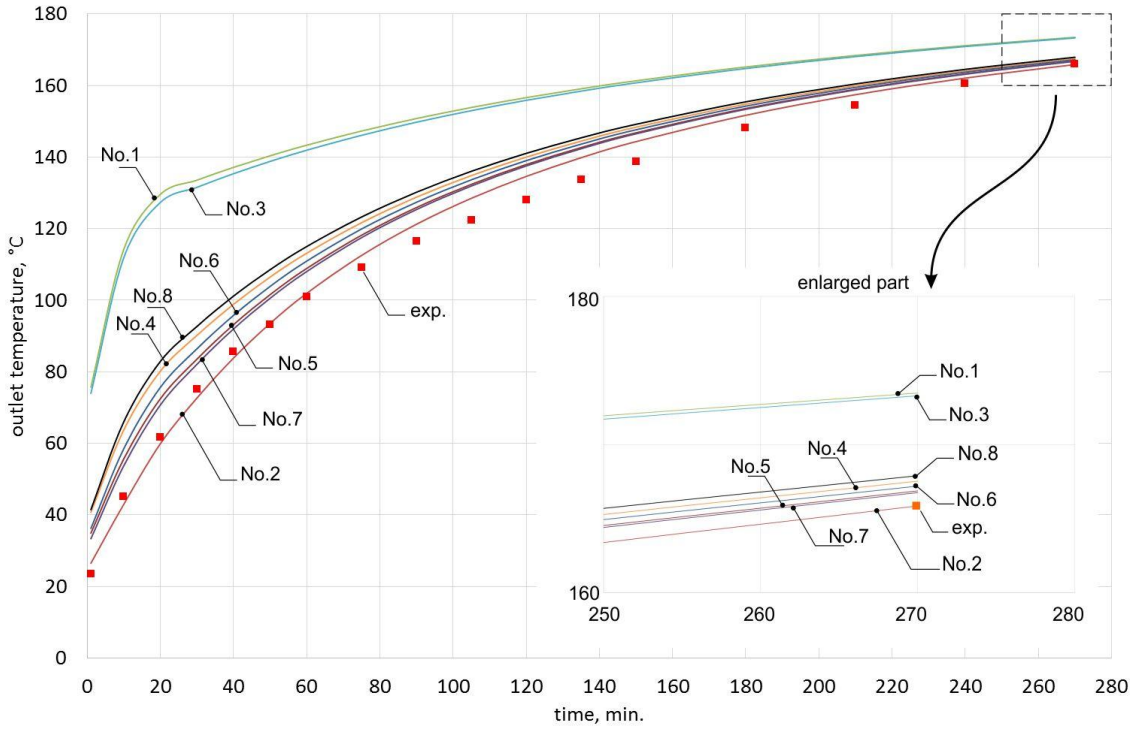

Figure 7. Outlet temperature for the airflow of 0.0068 m^3/s, for each of the dimensionless equations from Table 2.

Analysis of the Thermo-Hydraulic Efficiency for the Heat Storage Process in Ceramic Bricks

Calculating the thermo-hydraulic efficiency for the charging process required the measurement of pressure drops in the system. These were 1.7 Pa for the airflow of 0.0050 m^3/s, and 3.0 Pa for the

airflow of 0.0068 m^3/s. The analytically determined pressure drops were, respectively, 1.8 Pa and 3.3 Pa. Efficiencies were calculated from Equation (4). The model results, along with the experimentally obtained data and with uncertainty bars, are presented in Figures 8 and 9.

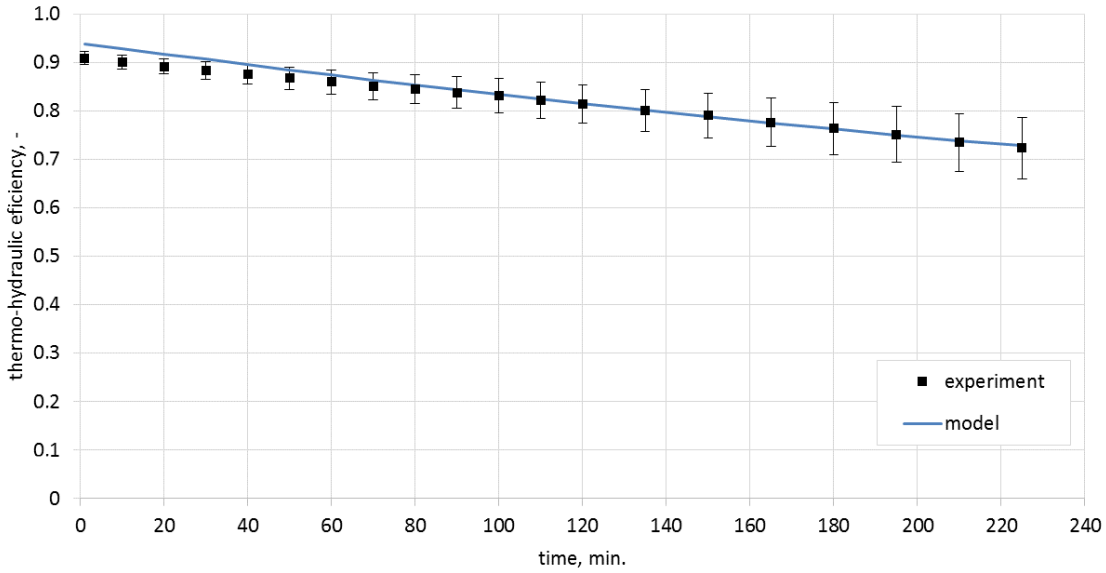

Figure 8. Thermo-hydraulic efficiency for the airflow rate of 0.0050 m^3/s.

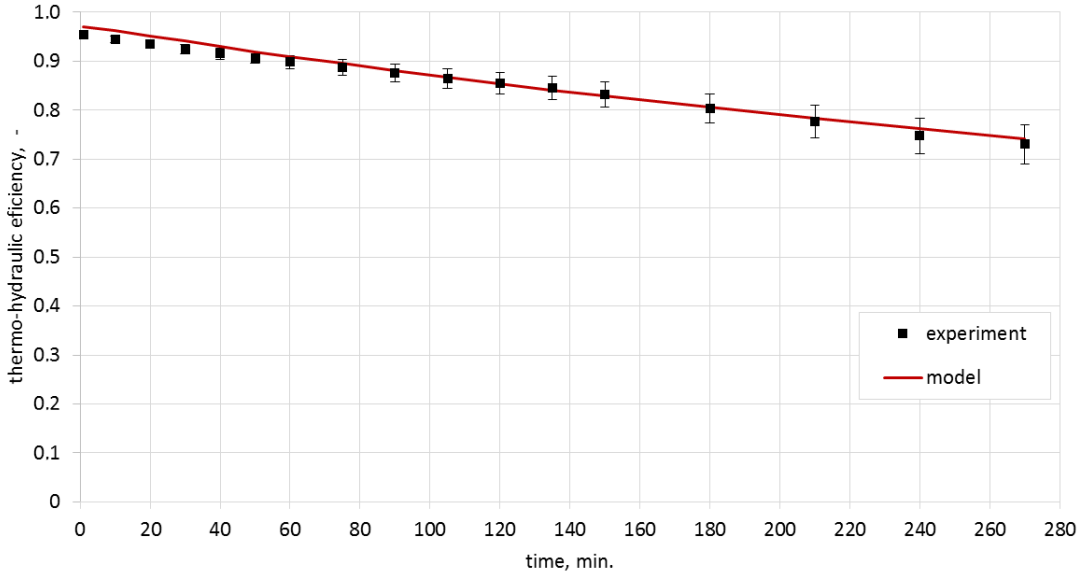

Figure 9. Thermo-hydraulic efficiency for the airflow rate of 0.0068 m^3/s.

The analysis of the obtained characteristics allowed concluding that the process of heat storage in ceramic brick has high efficiency which, during the experiment, was in the range of 72%–93% for the airflow rate of 0.0050 m^3/s and 74%–96% for the airflow rate of 0.0068 m^3/s.

As shown in Figure 10, one of the reasons for the change of efficiency in time is the change of the difference between the inlet temperature and the ceramic brick temperature. Notably, the thermo-hydraulic efficiency was over 70% already for the lowest temperature differences recorded during the experiment. As can be observed in Figure 9, process efficiency for lower temperature differences can be still maintained at a constant level by limiting the airflow rate. This fact is of great importance if the storage device is integrated with a heat source of variable intensity.

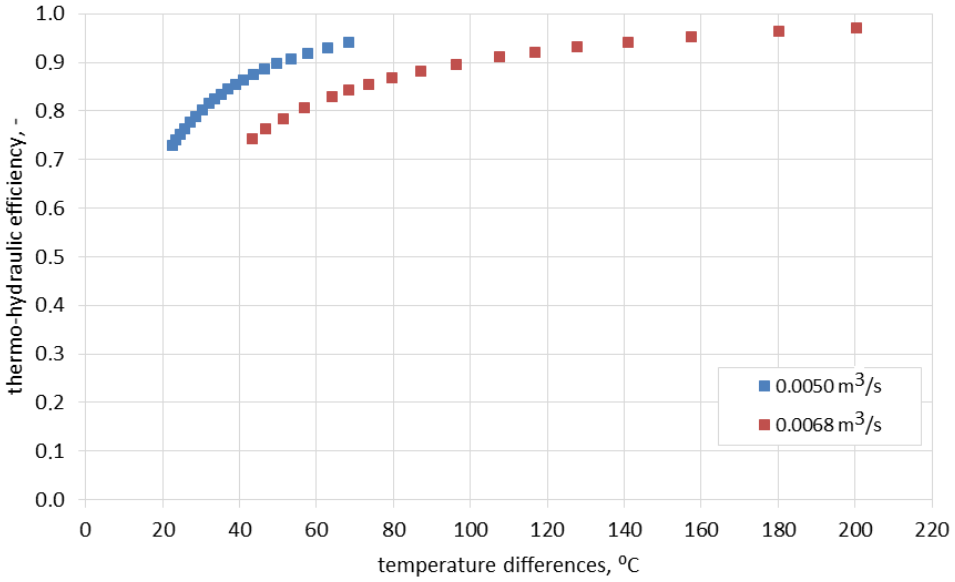

Figure 10. Thermo-hydraulic efficiency as a function of the difference between the inlet temperature and ceramic brick temperature.

In order to estimate the influence of airflow rate on the efficiency of the process, the model was used to calculate the characteristics for four inlet temperatures as a function of airflow rate and various ceramic brick temperatures (Figures 11–14).

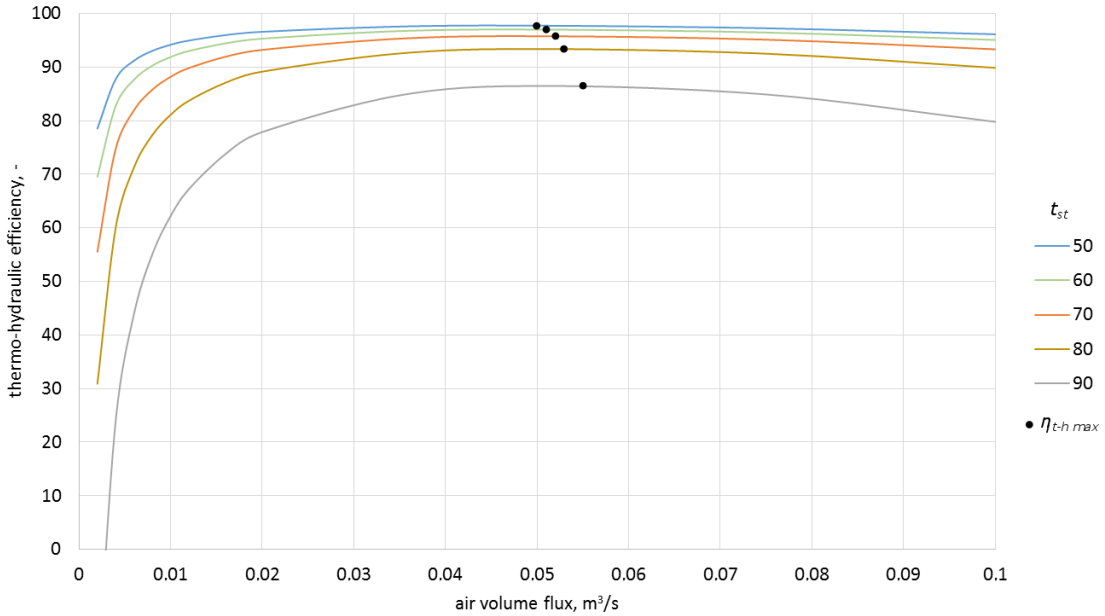

Figure 11. Thermo-hydraulic efficiency for the inlet temperature of 100 °C and various ceramic brick temperatures.

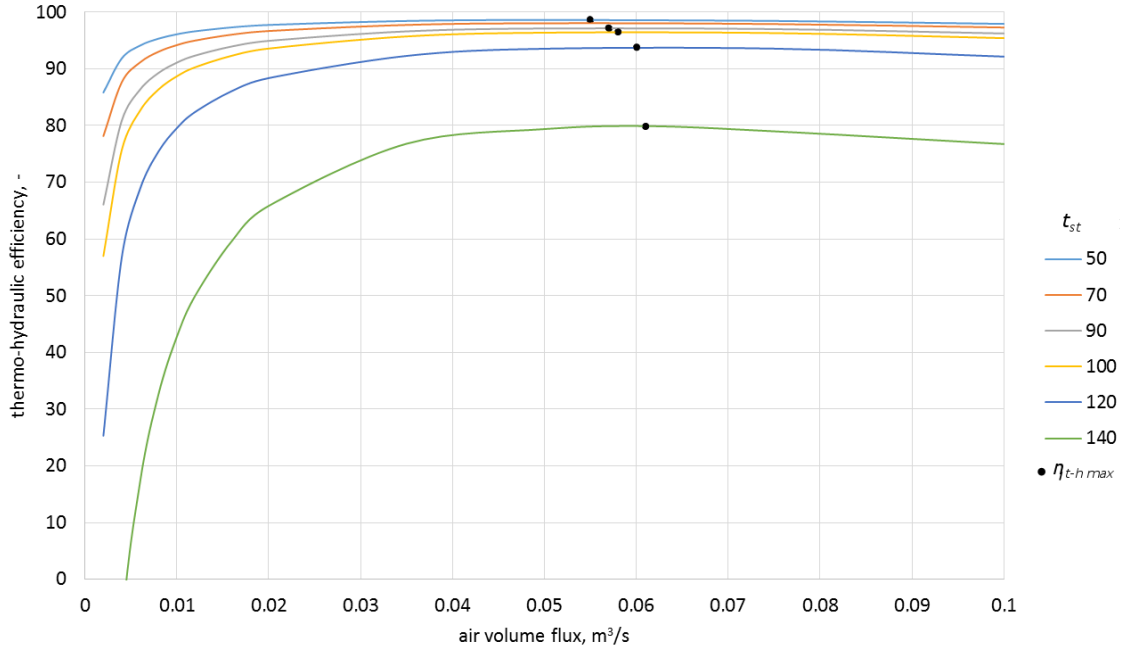

Figure 12. Thermo-hydraulic efficiency for the inlet temperature of 150 °C and various ceramic brick temperatures.

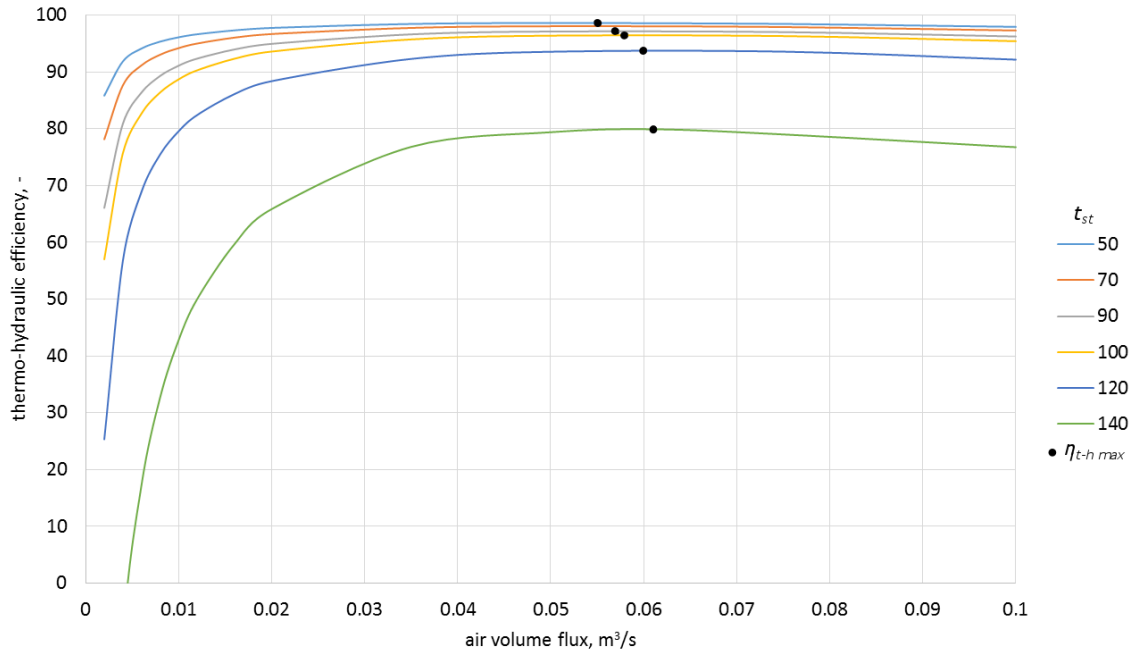

Figure 13. Thermo-hydraulic efficiency for the inlet temperature of 200 °C and various ceramic brick temperatures.

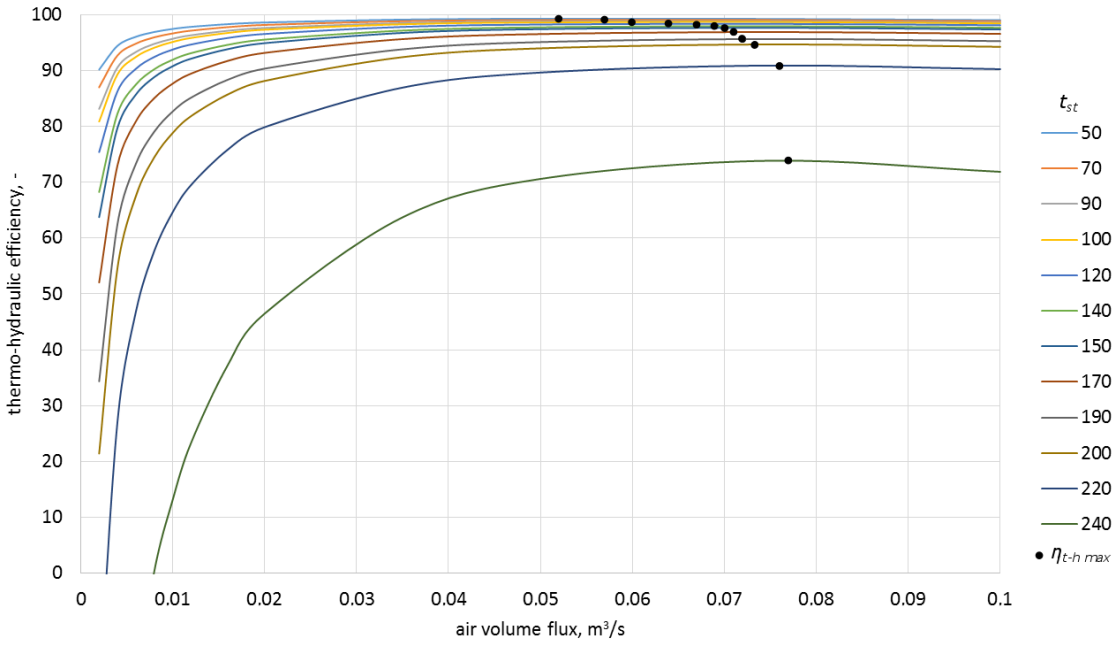

Figure 14. Thermo-hydraulic efficiency for the inlet temperature of 250 °C and various ceramic brick temperatures.

As can be observed in the above graphs, the thermo-hydraulic efficiency in the analyzed packed bed exceeds 90% for a wide range of airflow rates. The appropriate difference between the inlet temperature and ceramic brick temperature is of importance. For the inlet temperature of up to 150 °C, this difference needed to exceed 20 °C, while for the temperatures between 150 °C and 250 °C, the difference needed to exceed 30 °C. In the analyzed case, the thermo-hydraulic efficiency reaches maximal value for airflow rate of approximately 0.05 m^3/s. The $\eta_{t-h\ max}$ occurs when the airflow rate increases and the difference between the inlet temperature and the ceramic brick temperature decreases. The decrease in the thermo-hydraulic efficiency for greater airflow rates is caused by increasing pressure loss.

6. Conclusions

The thermo-hydraulic efficiency reaches maximal value for certain airflow rates and temperature difference. Such a maximum does not occur for the thermal efficiency, which increases together with increasing airflow rate. This is caused by the rapidly increasing pressure drop accompanied by the increasing speed of the working medium. The above fact means that the thermo-hydraulic efficiency is a good indicator of the economic effectiveness of the process.

As demonstrated in the above analyses, a system in which heat is stored in a sensible heat storage material, such as ceramic brick, should be provided with a means to control airflow rate in order to maximize the effectiveness of heat storage process, if the heat comes from a source of variable intensity, such as a concentrated solar air collector.

The developed model of the process of heat storage in a sensible heat storage material such as ceramic brick allows a precise description of heat storage phenomenon. The research results presented in this article are intended to aid the verification of a concept of using a sensible heat storage device coupled with a solar air heater, which may ensure thermal self-sufficiency to a residential house on a yearly basis. Therefore, the analyses in the next stage of research will cover the cooperation of the previously examined experimental set-ups with the solar collector and the packed bed to verify the assumed concept.

Acknowledgments: This work is sponsored by Ministry of Science and Higher Education in Poland under the grant for Wroclaw University of Science and Technology. Project No 0402/0232/16.

Author Contributions: Magdalena Nemś conceived and designed the experiments, analyzed the data and designed the model; Jacek Kasperski designed the set-up; Artur Nemś analyzed the data and developed a heat exchange model; and Michał Pomorski developed a heat exchange model.

Conflicts of Interest: The authors declare no conflict of interest.

References

1. Starr, C.H. Global energy and electrical futures. *Energy* **1993**, *18*, 33–39. [CrossRef]
2. Cabeza, L.F. *Surplus Heat Management Using Advanced TES for CO_2 Mitigation*; Final report, Annex 25; Energy Conservation through Energy Storage (ECES IA): Paris, France, 2011.
3. Mehling, H.; Cabeza, L.F. *Heat and Cold Storage with PCM*; Springer: Berlin, Germany, 2008.
4. Chandra, P.; Willits, D.H. Pressure drop and heat transfer characteristics of air-rockbed thermal storage systems. *Sol. Energy* **1981**, *27*, 547–553. [CrossRef]
5. Sagara, K.; Nakahara, N. Thermal performance and pressure drop of rock beds with large storage materials. *Sol. Energy* **1991**, *47*, 157–163. [CrossRef]
6. Meier, A.; Winkler, C.; Wuillemin, D. Experiment for modeling high temperature rock bed storage. *Sol. Energy Mater.* **1991**, *24*, 255–264. [CrossRef]
7. Garg, H.P.; Bandyopadhyay, B.; Sharma, V.K. Investigation of rock bed solar collector cum storage system. *Energy Convers. Manag.* **1981**, *21*, 275–282. [CrossRef]
8. Allen, K.G.; Von Backstrom, T.W.; Kroger, D.G.; Kisters, A.F.M. Rock bed storage for solar thermal power plants: Rock characteristics, suitability, and availability. *Sol. Energy Mater. Sol. Cells* **2014**, *126*, 170–183. [CrossRef]
9. Zanganeh, G.; Pedretti, A.; Zavattoni, S.; Barbato, M.; Steinfeld, A. Packed-bed thermal storage for concentrated solar power—Pilot-scale demonstration and industrial-scale design. *Sol. Energy* **2012**, *86*, 3084–3098. [CrossRef]
10. Kurklu, A.; Bilgin, S.; Ozkan, B. A study on the solar energy storing rock-bed to heat a polyethylene tunnel type greenhouse. *Renew. Energy* **2003**, *28*, 683–697. [CrossRef]
11. Abbud, I.A.; Löf, G.O.G.; Hittle, D.C. Simulation of solar air heating at constant temperature. *Sol. Energy* **1995**, *54*, 75–83. [CrossRef]
12. Cortes, A.; Piacentini, R. Improvement of the efficiency of a Bare Solar Collector by means of turbulence promoters. *Appl. Energy* **1990**, *36*, 253–261. [CrossRef]
13. Mittal, V.; Kumar, T.S. First & Second Law Analysis of Solar Air Heater. *J. Technol. Innov. Renew. Energy* **2012**, *1*, 63–71. [CrossRef]
14. El-Sebaii, A.A.; Aboul-Enein, S.; Ramadan, M.R.I.; El-Bialy, E. Year round performance of double pass solar air heater with packed bed. *Energy Convers. Manag.* **2007**, *48*, 990–1003. [CrossRef]
15. Gupta, D.; Solanki, S.C.; Saini, J.S. Thermohydraulic performance of solar air heaters with roughened absorber plates. *Sol. Energy* **1997**, *61*, 33–42. [CrossRef]
16. Singh, S.; Dhiman, P. Thermal and thermohydraulic efficiency of recyclic-type double pass solar air heaters with fins and baffles. *Heat Transf. Eng.* **2016**, *37*, 1302–1317. [CrossRef]
17. Mittal, M.K.; Varshney, L. Optimal thermohydraulic performance of a wire mesh packed solar air heater. *Sol. Energy* **2006**, *80*, 1112–1120. [CrossRef]
18. Wisniewski, S.; Wisniewski, T.S. *Heat Transfer*; WNT: Warsaw, Poland, 2012.
19. Kostowski, E. *A Collection of Tasks with Heat Flow*; Silesian University of Technology: Gliwice, Poland, 2006.
20. Kasperski, J.; Nemś, M. Investigation of thermo-hydraulic performance of concentrated solar air-heater with internal multiple-fin array. *Appl. Therm. Eng.* **2013**, *58*, 411–419. [CrossRef]
21. Nemś, M.; Kasperski, J. Experimental investigation of concentrated solar air-heater with internal multiple-fin array. *Renew. Energy* **2016**, *97*, 722–730. [CrossRef]
22. Fernández, A.I.; Martínez, M.; Segarra, M.; Martorell, I.; Cabeza, L.F. Selection of materials with potential in sensible thermal energy storage. *Sol. Energy Mater. Solar Cells* **2010**, *94*, 1723–1729. [CrossRef]
23. Grabarczyk, C.Z. *Flows in Closed Conduits. Calculation Methods*; Envirotech: Poznan, Poland, 1997.
24. Jezowiecka-Kabsch, K.; Szewczyk, H. *Fluid Mechanics*; Publishing House of Wroclaw University of Science and Technology: Wroclaw, Poland, 2001.

25. Pelech, A. *Fundamentals of Air Conditioning and Ventilation*; Publishing House of Wroclaw University of Science and Technology: Wroclaw, Poland, 2013.
26. Domanski, R. *Storage of Heat Energy*; PWN: Warsaw, Poland, 1990.
27. Wakao, N.; Kaguei, S.; Funazkri, T. Effect of fluid dispersion coefficients on particle-to-fluid heat transfer coefficients in packed beds: Correlation of Nusselt numbers. *Chem. Eng. Sci.* **1979**, *34*, 325–336. [CrossRef]
28. Nield, D.A.; Bejan, A. *Convection in Porous Media*, 3rd ed.; Springer International Publishing: Cham, Switzerland, 2006.
29. Beasley, D.E.; Clark, J.A. Transient response of packed bed for thermal energy storage. *Int. J. Heat Mass Transf.* **1984**, *27*, 1659–1669. [CrossRef]
30. Singh, R.; Saini, R.P.; Saini, J.S. Nusselt number and friction factor correlations for packed bed solar energy storage system having large sized elements of different shapes. *Sol. Energy* **2006**, *80*, 760–771. [CrossRef]
31. Kline, S.; McClintock, F. Describing uncertainties in single-sample experiments. *Mech. Eng.* **1953**, *75*, 3–8.